Agricultural and Forest Meteorology 319 (2022) 108933

Contents lists available at ScienceDirect

Agricultural and Forest Meteorology

journal homepage: www.elsevier.com/locate/agrformet

Identifying sources of uncertainty in wheat production projections with consideration of crop climatic suitability under future climate

Tengcong Jiang [a,b,c], Bin Wang [d], Xijuan Xu [a,e], Yinxuan Cao [a,e], De Li Liu [d], Liang He [f], Ning Jin [c], Haijiao Ma [a,e], Shang Chen [a,e], Kuifeng Zhao [g], Hao Feng [c,e], Qiang Yu [c,g], Yingbin He [b,*], Jianqiang He [a,e,g,*]

[a] Key Laboratory for Agricultural Soil and Water Engineering in Arid Area of Ministry of Education, Northwest A&F University, Yangling, Shaanxi 712100, China
[b] Institute of Agricultural Resources and Regional Planning, Chinese Academy of Agricultural Sciences, Beijing 100081, China
[c] State Key Laboratory of Soil Erosion and Dryland Farming on the Loess Plateau, Institute of Water and Soil Conservation, Northwest A&F University, Yangling, Shaanxi 712100, China
[d] New South Wales Department of Primary Industries, Wagga Agricultural Institute, Wagga, New South Wales, Australia
[e] Institute of Water-Saving Agriculture in Arid Areas of China, Northwest A&F University, Yangling, Shaanxi 712100, China
[f] National Meteorological Center, Beijing 100081, China
[g] Key Laboratory of Eco-Environment and Meteorology for the Qinling Mountains and Loess Plateau, Shaanxi Provincial Meteorological Bureau, Xi'an, Shaanxi 710015, China

ARTICLE INFO

Keywords:
Winter wheat
Crop model
GCMs
Climate suitability
SDMs
Uncertainty

ABSTRACT

Climate change poses a great challenge to global food security. Recently the combination of crop models (CMs), global climate models (GCMs), and species distribution models (SDMs) has been applied to assess the impacts of climate change on crop production with consideration of changes of crop climate-suitable regions. However, little is known about the uncertainty sources in the wheat production projections with consideration of crop climatic suitability under future climate. In this study, an integration method based on multiple CMs, SDMs, and GCMs was adopted to assess the impacts of climate change on winter wheat production in the Loess Plateau of China. A comprehensive analysis of different uncertainty sources (i.e. CM, GCM, SDM, Emission Scenario or *Scen*, and their interactions) was conducted through the ANOVA (Analysis of variance) method. Based on the projections of CM ensemble and ensemble-SDMs driven by 27 GCMs, multi-model mean winter wheat production would increase by 14.6% and 19.7% in 2041–2060 and 4.9% and 3.5% in 2081–2100 under SSP245 and SSP585, respectively. We found that the changes in climate-suitable areas of winter wheat caused larger changes in winter wheat production than the changes of per unit yield. SDM was the largest uncertainty contributor among the four main factors of CM, GCM, SDM, and *Scen* in the projections of winter wheat production under future climate in the Loess Plateau, accounting for about 20.3% of total uncertainty. At the same time, CM was the lowest uncertainty contributor and accounted for only about 3.0% of total uncertainty. Thus, CM was proved more certain in future projections of winter wheat production when considering the changes of crop climate-suitable areas. The efforts in this study could help to rationally integrate the crop modeling, species distribution modeling, and climate models on the projections of global wheat production under future global climate change.

1. Introduction

Global population is expected to reach approximately 9.7 billion by 2050 (White and Gardea-Torresdey, 2018) and this steady growth is driving up food demand dramatically (van Dijk et al., 2021). Climate change has put great pressure on global food security since climate warming (Asseng et al., 2015; Zhao et al., 2017), seasonal uneven changed precipitation (Lesk and Coffel 2020), and climate extremes have significantly affected crop production (Chavez et al., 2015; Li et al., 2019). At the same time, land use attributes another part of accessibility and availability of this vital food source. Over the past ten years, rapid urbanization and widespread degradation of agricultural land have placed additional pressure on global food suply as the area of arable agricultural land declines (IPCC, 2019). In Australia, for example, any

* Corresponding authors.
E-mail addresses: heyingbin@caas.cn (Y. He), jianqiang_he@nwsuaf.edu.cn (J. He).

https://doi.org/10.1016/j.agrformet.2022.108933
Received 12 August 2021; Received in revised form 18 March 2022; Accepted 28 March 2022
Available online 6 April 2022

positive effects of climate change will be insufficient to prevent a likely decline in production under a high CO_2 emission scenario by 2081–2100 due to the increasing loss of suitable wheat growing areas (Wang et al., 2018). Nonetheless, in the northern hemisphere, cropping area expanded northward due to the rising temperatures (King et al., 2018; Ramirez-Cabral and Kumar, 2016). Thus, more research began to focus on agronomic strategies that could simultaneously maintain or even increase crop per unit yield in climate-suitable regions under climate change so as to ensure future food security (Senapati et al., 2019; Tanaka et al., 2015; Wang et al., 2018).

Winter wheat, one of the world's staple food crops, is experiencing a production decline of about 5.5% due to climate change in the past a few decades (Lesk et al., 2016; Lobell et al., 2011), in spite of the improvements in genetic technology and agronomic management (Ortiz-Bobea et al., 2021). Moreover, climate change could both shift the characteristics of wheat growth and development (Asseng et al., 2015; Corbeels et al., 2018; He et al., 2015) and alter their spatial distributions (Manners and Varela-Ortega, 2020; Wang et al., 2018; Wheeler, 2013). In China, for instance, the expanding of northern borders of cropping systems contributed about 2.2% increase to national production of major crops (Yang et al., 2015). On the contrary, a decline in the areas suitable for growing wheat have been projected in the Australian under future climate change (Wang et al., 2018).

Usually, statistical-based models (Lobell et al., 2011; Zhao et al., 2016), process-based biological crop models (CMs) (Asseng et al., 2015; Wang et al., 2017), and their combinations (Feng et al., 2020, 2019) were used as robust tools to investigate the impacts of climate change on main crop yields worldwide with projected climatic data from multiple global climate models (GCMs). Especially, the process-based biological crop models have been a common tool for getting insights into the impacts of climate change on agricultural production system (Basso et al., 2021; Liu et al., 2021). However, inconsistencies among crop models in the interactions of temperature, atmospheric CO_2 emissions, and seasonal rainfall might lead to opposite trend of in predicted crop yields under future climate change (Wang et al., 2020), which could cause larger uncertainty in the projections. Asseng et al. (2013) reveled that the larger proportion of uncertainty was contributed by crop models than by downscaled GCMs in their projections of climate change impacts on crop yield. In addition, the identification of uncertainty sources had extended to crop model parameters and managements (Tao et al., 2018; Xiong et al., 2019). Furthermore, Xiong et al. (2019) explored the global geographic pattern of total uncertainty in climate change impact projections and found that low latitudes had lower uncertainty than middle and high latitudes. Nonetheless, site-specific sources of uncertainty in the projections of climate change impacts were also highlighted by Wang et al. (2020). Thus, there are still some knowledge gaps in identifying the dominating sources of uncertainty in crop yield projections under future climate change.

The spatial distributions of species under the suitable environmental conditions (e.g. temperature and rainfall) can be modeled by the species distribution models (SDMs) (Araújo et al., 2019; Elith and John, 2009). Recently, possible distributions of field crops (maize, wheat, bean) have been projected by SDMs with historical or future climate data at global and country scales (He, 2016; He et al., 2019; Ramirez-Cabral and Kumar, 2016; Sun and Zhou, 2012). It was noteworthy that the combination of CMs, GCMs, and SDMs had already been used to assess the impacts of climate change on crop production at country scale. For instance, Wang et al. (2018) applied multiple SDMs to investigate the changes of climate-suitable areas for wheat production under future climate change. They then used the Apsim model to assess the change of per unit yield in these areas and projected whole wheat production in Australia. Sources of uncertainties in the projections of crop grain yield and spatial distributions under climate change were also discussed by several other research (Asseng et al., 2013; Stoklosa et al., 2015; Tao et al., 2018; Thuiller et al., 2019). However, little is known about the contributions of various sources (i.e. GCM, CM, SDM, Emission Scenario or *Scen*, and their interactions) to the total uncertainty in the projections of winter wheat production with consideration of the changes in climate-suitable areas under future climate.

In this study, we selected the Loess Plateau as a representative region in China, where wheat production is vulnerable to climate change, to simulate its winter wheat production with six different CMs, nine SDMs, and 27 GCMs under four future climate change scenarios (i.e. 2041–2060_SSP245, 2041–2060_SSP585, 2081–2100_SSP245, and 2081–2100_SSP585) based on the Coupled Model Intercomparison Project phase 6 (CMIP6). The objectives were (1) to investigate the changes of per unit yield and climate-suitable areas of winter wheat in the Loess Plateau under future climate, (2) to assess the changes of regional production of winter wheat under future climate, and (3) to identify the sources of uncertainties in the projections of winter wheat production influenced both by the changes of per unit yield and climate-suitable areas under future climate change.

2. Materials and methods

2.1. Study area

The Loess Plateau is of one the most ecologically vulnerable areas and typical dryland farming areas in China (Jin et al., 2018). Winter wheat is mainly cultivated in northern Henan province, Shanxi province, Shaanxi province, southeastern Gansu province, and southern Ningxia province in China. Winter wheat cultivation mainly depends on rainfall and is very vulnerable to the climate change in this region. In the Loess Plateau, wheat accounts for about 21.2% of national wheat planting area (3.47±0.96 million hectares) and 9.3% of national wheat production (11.81±1.85 million tons) (Fig. S1). Mean daily temperature in winter wheat growing season (September of sowing year to June of harvest year) rose from north to south, with a mean value of −4∼12 °C (Fig. 1b) in 1971–2010. Averaged cumulative rainfall in winter wheat growing season (160∼500 mm) shared the similar spatial pattern with mean temperature (Fig. 1c). Nonetheless, mean cumulative radiation in winter wheat growing season (2500∼4500 MJ m^{-2}) declined from north to south (Fig. 1d). Based on the remotely sensing survey data from Jin et al. (2018), winter wheat cultivation areas were mainly distributed in southern Shanxi province, central Shaanxi province, and southeast of Gansu province (green pixels in Fig. 1a). These three provinces differed in winter wheat management options, such as wheat cultivar, plant date, plant density, and fertilization rates (He et al., 2014). Moreover, in winter wheat cultivation regions in the Loess Plateau, averaged daily temperature and cumulative rainfall decreased from east to west. Thus, we divided the whole planting areas of winter wheat into three subregions (i.e., Subregion I, II, and III) from east to west in the Loess Plateau (Fig. 1a), which was more convenient for crop model simulation.

2.2. Climate, soil, and experimental data

Daily weather data (maximum and minimum temperatures, rainfall, and solar radiation) were obtained from the National Meteorological Information Center (http://data.cma.cn/) for the 297 national weather stations located in the Loess Plateau in 1971–2010 (baseline). Future climate in periods of 2041–2061 and 2081–2100 of each weather station were obtained from 27 different GCMs (Table S1). Additionally, to investigate the relative change in future projections, climatic data in 1971–2010 were also attained from the GCMs. The weather data from the 27 GCMs were spatiotemporally downscaled to daily scale for the 297 national weather stations located in the Loess Plateau (Fig. 1a). Details about the description of the downscaling method can be found in Liu and Zuo (2012). This method has been widely applied in recent climate change impact studies in Australia (Wang et al., 2020, 2017) and China (Ruan et al., 2018; Xiao et al., 2020).

The soil data used in the simulations with six different CMs (Table S2) in this study included soil physical parameters (i.e. saturated

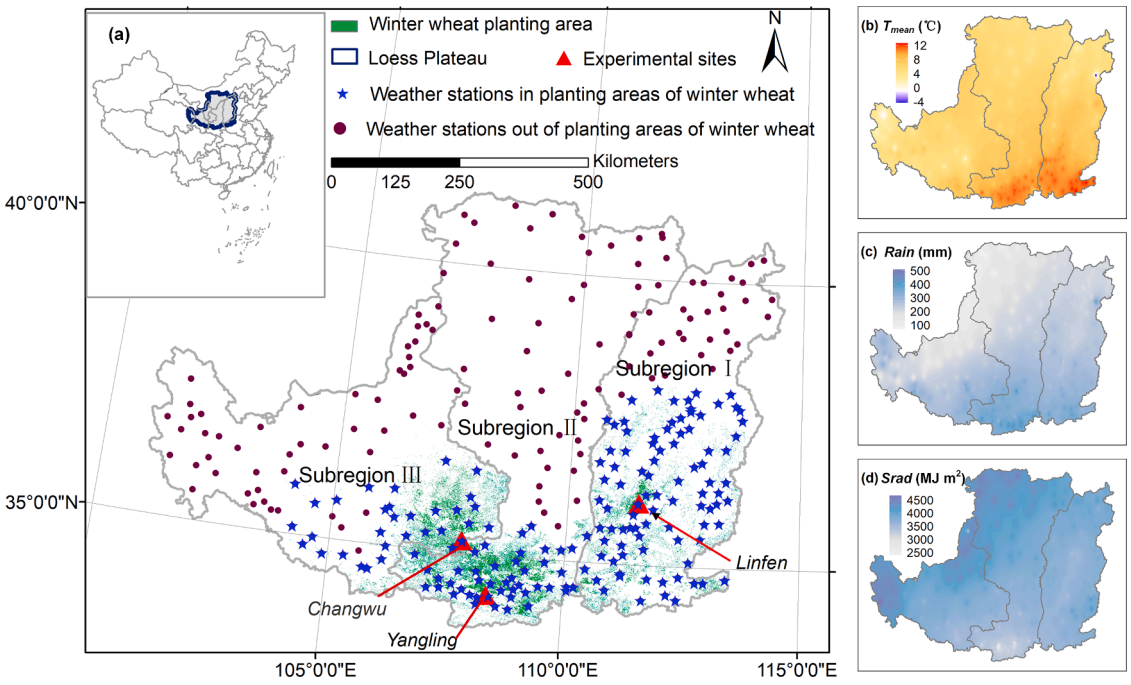

Fig. 1. Spatial distributions of winter wheat cultivation areas, three experimental sites for model calibration and validation (*Linfen, Yangling, Changwu*; three red filled triangles), national weather stations (166 blue filled pentagrams in the current planting areas and 131 brown filled circles out of the current planting areas of winter wheat), three subregions of winter wheat planting areas (a), with the mean temperature (b; ℃), mean cumulative rainfall (c; mm), and mean cumulative solar radiation (d; MJ m^{-2}) from September of sowing year to June of harvest year of winter wheat in the Loess Plateau of China. Sub-region I: northwestern Henan Province and Shanxi Province; Sub-region II: middle and northern Shaanxi Province and southern Inner Mongolia; and Sub-region III: southeastern Gansu Province, eastern Qinghai Province, and southern Ningxia Province.

moisture content, field capacity, and wilting point), bulk density, organic carbon, and pH at soil depths (Table S3). The SDMs variables related to soil physical and chemical properties were obtained from the Chinese soil hydrographic dataset (http://westdc.westgis.ac.cn) (Dai et al., 2013) and the HWSD (Harmonized World Soil Database version 1.1 HWSD) dataset (Wieder et al., 2014).

With consideration of the temperature differences in the three subregions (Fig. 1a), three mainly cultivated winter wheat cultivars with different life cycles were selected as representative cultivars in the three subregions. The field experiments with the longest growing season of winter wheat were conducted at the Changwu Agro-ecological Experiment Station in Shaanxi Province (35°14′ N, 107°41′E, 1220 m), where the sowing dates were Sept.−25 in 2004, Sept.−26 in 2005, Sept.−21 in 2007, and Sept.−17 in 2008, respectively. Cultivars of the experiments were '*Changwu 89,134*' in the 2004–2006 growing seasons and '*Changhan 58*' in the 2007–2009 growing seasons (Table S4). More basic data of the eight-year field experiments and information about soil properties of the experimental site at Changwu were reported in Ding et al. (2016). The field experiment with the shortest growing season of winter wheat was conducted under rainout shelters between 2012 and 2013 at the Key Laboratory for Agricultural Soil and Water Engineering in Arid Area of Ministry of Education of Northwest A&F University at Yangling in Shaanxi Province (34°17′N, 108°04′E, 506 m), where the cultivar was '*Xiaoyan 22*' and the sowing dates were Otc-15 in 2012 and Oct.−15 in 2013 (Table S4). More details about the experiments can be found in Yao et al. (2015). The rest of the experiments were conducted in 2008–2015 under rainfed conditions at Linfen in Shanxi Province (36°5′N, 111°45′E, 693.5 m) with a winter wheat cultivar of '*Linfen 45*'. The experimental factors included planting date and density (Table S4). The fertilizer application rate was the same for all treatments, with a base fertilizer of 150 kg N ha^{-1} and 50 kg P_2O_5 ha^{-1}. Fertilizer application date was set as the day before sowing. More experimental details can be found in Pei et al. (2017).

2.3. Crop model setting under various emission scenarios

The relevant parameters of the six crop models (i.e. Apsim, AquaCrop, DSSAT-CERES-Wheat, DSSAT-CSCRP-Wheat, DSSAT-NWheat, and STICS) were obtained through the processes of model calibration and validation (Tables S5–10). Because the six crop models did not have unified tools for parameter optimization. Thus, calibration and validation of the six crop models were conducted based on the least square method in R language. Then, the six validated crop models were used to simulate the phenology dates and per unit grain yield of winter wheat with observed climatic data (1971–2010) and downscaled climatic data (1971–2010, 2041–2060, and 2081–2100) with the 27 GCMs under SSP245 and SSP585 scenario across 166 weather stations in the Loess Plateau (Fig. 1a). The initial soil water content was reset as 75% of plant available water on August 1th. Then, the initial nitrogen contents in 1 m soil profile were reset as 80, 70, and 60 kg N ha^{-2} in Subregion I, Subregion II, and Subregion III, respectively. All simulation scenarios were set under rainfed condition, with planting densities of 300, 300, and 500 plant m^{-2} in the three subregions. According to local farmers' management practices, the fertilizer schedules of 150 N 60 P 30 K kg ha^{-2}, 120 N 80 P 40 K kg ha^{-2}, and 160 N 40 P 30 K kg ha^{-2} were set in the three subregions, respectively. The planting dates were automatically triggered at 40% of plant available water in 0–30-cm soil layer. Sowing widows were set as September 10th-October 20th, September 20th-October 20th, and September 20th-October 10th in the three subregions, respectively. Moreover, the response of crop to atmospheric CO_2 concentration was considered and fitted for scenario SSP245 (Eq. (1)) and SSP585 (Eq. (2)) based on the projection data from the SSP database (Gidden et al., 2019). Multi-CM ensemble mean was calculated based on the projections of the six CMs. The simulation results based on historical weather data were used to calculate the relative changes for simulation variables based on the downscaled climatic data of the 27 GCMs.

$$[CO_2]_{year} = 62.044 + \frac{34.002 - 3.8702 \times y}{0.24423 - 1.1542 \times y^{2.4901}} + 0.028057 \times (y - 1900)^2 + 0.00026827 \times (y - 1960)^3 - 9.2751 \times 10^{-7} \times (y - 1910)^4 - 2.2448 \times (y - 2030) \quad (1)$$

$$[CO_2]_{year} = 757.44 + \frac{84.938 - 1537 \times y}{2.2011 - 38289 \times y^{-0.45242}} + 2.4712 \times 10^{-4} \times (y + 15)^2 + 1.9299 \times 10^{-5} \times (y - 1937)^3 + 5.1137 \times 10^{-7} \times (y - 1910)^4 \quad (2)$$

2.4. Simulation of climate-suitable area for winter wheat

Generally, the species distribution models (SDMs) are used to establish statistical relationship between species '*presences*', '*absences*', and environmental variables (e.g. temperature, precipitation, soil, vegetation, and etc.) to determine the environmental conditions required for species survival. The variables of '*presences*' and '*absences*' represent the spatial distributions of climate-suitable and climate-unsuitable locations in the SDMs. Based on latitude and longitude of '*presences*' and '*absences*', environmental data were extracted as inputs to train and test the models. '*Presences*' and '*absences*' were encoded as '1′ and '0′, which were dependent variables in model training and testing. Then, after model testing, the SDMs could estimate the spatial and temporal distributions of species survival possibility, forced by the spatial environmental data. Researchers usually refer to a threshold to determine the acreage distribution of predicted spatial species survival possibility.

In this study, climate-suitable areas of winter wheat were simulated with nine widely used species distribution models (SDMs), including GAM, GBM, Glmnet, Maxlike, MLP, SVM, RBF, RF, and RPART (Table S11). The nine SDMs are integrated in the '*sdm*' package in R language (Naimi and Miguel, 2016). In addition, a total of 20 different environment variables (Table S12) related to winter wheat growth and development were used in the projections of climate-suitable areas with various SDMs.

2.4.1. Training and testing processes of SDMs

A bootstrapping procedure was used to train and test the involved SDMs with '*sdm*' package (Naimi and Miguel, 2016). All of the nine SDMs need '*presences*' and '*absences*' to determine the suitable conditions for winter wheat production across the whole research region. To determine the spatial distributions of '*presences*' and '*absences*', random spatial sampling with a sample size of 2000 was executed through the '*sdm*' package in R language. Then, '*presences*' were obtained within the 891 locations in the cultivation areas of winter wheat surveyed by Jin et al. (2018). And, '*absences*' were the rest 1109 locations out the cultivation areas of winter wheat but still in the Loess Plateau. In order to reduce the random errors in SDMs simulations, each simulation was repeated ten times in the training and testing processes for the nine different SDMs according to the bootstrapping procedure. The model's performances in training and testing were quantified with AUC, (the area under the ROC curve, Eq. (3)), TSS (the true skill statistic, Eq. (4)), and COR (Pearson correlation coefficient, Eq. (5)).

$$\begin{cases} \mathrm{AUC} = 1 - \dfrac{1}{m^+ \times m^-} \sum_{x^+ \in D^+} \sum_{x^- \in D^-} (W(f(x^+) - f(x^-))) \\ W(f(x^+) - f(x^-)) = 1,\ f(x^+) \geq f(x^-) \\ W(f(x^+) - f(x^-)) = 0,\ f(x^+) < f(x^-) \end{cases} \quad (3)$$

where, m^+ and m^- were sample size marked as 1 and 0; D^+ and D^- were the sets marked as 1 and 0; x^+ and x^- were the sample marked as 1 and 0; $f(x^+)$ and $f(x^-)$ were the model predicted values under a given threshold.

$$\begin{cases} TPR = \dfrac{TP}{TP + FN} \\ TNR = \dfrac{TN}{FP + TN} \\ TSS = TPP - FRP - 1 \end{cases} \quad (4)$$

where, *TP, FN, FP*, and *TN* were true positive, false negative, false positive, and true negative cases predicted by the models under a given threshold, respectively; *TPN* and *TRN* were sensitivity and specificity.

$$COR = \frac{\sum_{i=1}^{n}(x_i - \bar{x}) \times (f(x_i) - \overline{f(x)})}{\sqrt{\sum_{i=1}^{n}(x_i - \bar{x})^2} \times \sqrt{\sum_{i=1}^{n}(f(x_i) - \overline{f(x)})^2}} \quad (5)$$

where x_i, and $f(x_i)$ were the observed and predicted values; $\bar{x}$, and $\overline{f(x)}$ were the mean of observed and predicted values

2.4.2. Predictions of climate-suitable areas of winter wheat with SDMs

First, multi-year mean climate related variables (Table S12) from observed climatic data in 1971–2010 and downscaled climatic data of 27 GCMs in 1971–2010, 2041–2061, and 2081–2100 under both emission scenarios across 297 weather stations were interpolated to resolution of 1 km using the inverse distance weighting method in the '*raster*' package of R. In order to meet the uniform resolution of SDMs inputs, the inputs related to topography and soil physical and chemical were resampled to the same resolution as climate related variables. Then the environmental variables (Table S12) were used to run the nine different validated SDMs. The predictions with each of the nine validated SDMs were the mean values of the corresponding ten repeat runs for each of the nine validated SDMs.

Standard deviations of TSS (true skill statistic) values were between that of AUC and COR in the testing process (Table S13). In order to rationally integrate results of the nine SDMs to an ensemble-SDMs value, the weights of different SDMs were calculated as the ratios between TSS of corresponding SDMs and sum of TSS. Then, the predictions of weighted-ensemble SDMs were calculated for current and future conditions based on the 27 GCMs. The SDMs-predicted survival possibility or climate suitability of winter wheat ranged 0–1 in each pixel in 1971–2010, 2041–2060, and 2081–2100 based on the 27 GCMs under both SSP245 and SSP585 scenarios. In this study, we set 0.5 as the threshold value to determine the '*presences*' and '*absences*' for all projections. Thus, we could obtain climate-suitable areas of winter wheat predicted by nine individual SDMs in different time windows. However, the projections were climate-suitable areas rather actual areas of winter

wheat in various time windows in the Loess Plateau. Thus, SDMs might estimate the spatial temporal distribution of the species survival possibility in forest, residential, grass, and etc. Thus, taking into account the bias between the simulated acreage and the statistical acreage, a correction method provided by Wang et al. (2018) was used to correct the predicted climate-suitable areas according to the statistical areas of winter wheat cultivation in the China Statistical Yearbook (2007–2014) (Eq. (6)). The correction factors (Table S14) obtained were therefore used to calculate the acreage of climate-suitable areas under future climate change.

$$\begin{cases} Factor = \dfrac{Areas_{SDM\_baseline}}{Areas_{China\ NBOSO}} \\ Areas_{SDM\_future} = \dfrac{Areas_{SDM\_future\ projection}}{Factor} \end{cases} \quad (6)$$

where *Factor*was the correction factors for the climate-suitable areas of winter wheat predicted by nine individual species distribution models (SDMs);$Areas_{SDM_baseline}$was multi-year mean climate-suitable areas of winter wheat predicted by SDMs in the baseline (1971–2010) with observed climate data, million hectare;$Areas_{ChinaNBOSO}$ was statistical areas of winter wheat cultivation in the China Statistical Yearbook (2007–2014), million hectare;$Areas_{SDM\_future}$ was the corrected multi-year mean climate-suitable areas of winter wheat predicted by SDMs under four future climate change scenarios, million hectare;$Areas_{SDM\_future\ projection}$ was the uncorrected multi-year mean climate-suitable areas of winter wheat predicted by SDMs under four future climate change scenarios, million hectare.

2.5. Projections of regional production of winter wheat

The projections of regional production of winter wheat were based on the predictions of per unit yields of winter wheat with six CMs and CM ensemble and the projections of climate-suitable areas of winter wheat with nine SDMs and weighted-ensemble SDMs driven by observed climatic data and downscaled climatic data from the 27 GCMs. The regional production of winter wheat projected by the combination of six CMs, CM ensemble, nine SDMs, weighted-ensemble SDMs, and 27 GCMs under four change scenarios (*Scen*) in the Loess Plateau and three sub-regions (*Reg*), or $[Produncrion\ {}^{Reg}_{GCM\_Scen}]^{SDM}_{CM}$ (million tons) was the product of the average per unit yield $[Yield^{Reg}_{GCM\_Scen}]_{CM}$ (kg ha^{-1}) projected by the corresponding combination of CMs, GCMs, *Reg* and *Scen* and the climate-suitable areas $[Areas^{Reg}_{GCM\_Scen}]_{SDM}$(million hectare) projected by the corresponding combination of SDMs, GCMs, *Reg*, and *Scen* (Eq. (7)).

$$\begin{aligned} T_{production} = {} & P_{production,\ CM} + P_{production,\ GM} + P_{production,\ SDM} + P_{production,\ Scen} + \\ & P_{production,\ CM\times GCM} + P_{production,CM\times SDM} + P_{production\ ,CM\times Scen} + \\ & P_{production,\ GCM\times SDM} + P_{production,\ GCM\times Scen} + P_{production,\ SDM\times Scen} + \\ & P_{production,\ CM\times GCM\times SDM} + P_{production,\ CM\times GCM\times Scen} + P_{production,\ CM\times SDM\times Scen} + \\ & P_{production,\ GCM\times SDM\times Scen} + P_{production,\ CM\times GCM\times SDM\times Scen} \end{aligned} \quad (10)$$

Additionally, the percentage was calculated as the ratio between the absolute change of production in 2041–2060 and 2081–2100 compared to 1971–2010 under SSP245 and SSP585 and production driven by observed climatic data.

$$\left[Produncrion\ {}^{Reg}_{GCM\_Scen} \right]^{SDM}_{CM} = \left[Yield\ {}^{Reg}_{GCM\_S_{Cen}} \right]_{CM} \times \left[Areas\ {}^{Reg}_{GCM\_Scen} \right]_{SDM} \quad (7)$$

2.6. Identification of uncertainty sources in yield, areas, and production projections

The contributions by different sources to the uncertainties in the projections of per unit yield, climate-suitable areas, and regional production of winter wheat were analyzed in the Loess Plateau under future climate change. First, three-way ANOVA analysis was conducted to assess the uncertainties in projected per unit yields caused by six CMs, 27 GCMs, four change scenarios, and their interactions (Eq. (8)). Next, the same method was used to assess the uncertainties in projected climate-suitable areas (Eq. (9)). Finally, four-way ANOVA analysis was conducted to analyze the uncertainties in projected regions production of winter wheat, taking into account a total of 15 uncertainty sources (Eq. (10)).

$$\begin{aligned} T_{yield} = {} & P_{yield,\ CM} + P_{yeld,\ GCM} + P_{yield,\ Scen} + P_{yield,\ CM\times\ Scen} + \\ & P_{yield,\ CM\times GCM} + P_{yield,\ GCM\times Scen} + P_{yield,\ CM\times GCM\times\ Scen} \end{aligned} \quad (8)$$

$$\begin{aligned} T_{areas} = {} & P_{areas,\ SDM} + P_{areas,\ GCM} + P_{areas,\ Scen} + P_{areas,\ SDM\times Scen} + \\ & P_{areas,\ SDM\times GCM} + P_{areas,\ GCM\times Scen} + P_{areas,\ SDM\times GCM\times Scen} \end{aligned} \quad (9)$$

where T_{yield} was the total uncertainty in projected per unit grain yields of winter wheat under future climate change; $P_{yield,CM}$, $P_{yield,GCM}$, $P_{yield,Scen}$, $P_{yield,CM\times Scen}$, $P_{yield,CM\times GCM}$, $P_{yield,GCM\times Scen}$, and $P_{yield,CM\times GCM\times Scen}$were the proportions of uncertainty contributed by CM (crop model), GCM (Global climate model), *Scen* (Emission Scenario), and their interactions; T_{areas} was the total uncertainty in projected climate-suitable areas under future climate change; $P_{areas,SDM}$, $P_{areas,GCM}$, $P_{areas,Scen}$, $P_{areas,SDM\times Scen}$, $P_{areas,SDM\times GCM}$, $P_{areas,GCM\times Scen}$, and $P_{areas,SDM\times GCM\times Scen}$were the proportions of uncertainty contributed by SDM (Species distribution model), GCM, *Scen*, and their interactions; $T_{production}$ was the total uncertainty in projected regional production of winter wheat under future climate change; $P_{production,CM}$, $P_{production,GCM}$, $P_{production,SDM}$, $P_{production,Scen}$, $P_{production,CM\times GCM}$, $P_{production,CM\times SDM}$, $P_{production,CM\times Scen}$, $P_{production,GCM\times SDM}$, $P_{production,GCM\times Scen}$, $P_{production,SDM\times Scen}$, $P_{production,CM\times GCM\times SDM}$, $P_{production,CM\times GCM\times Scen}$, $P_{production,CM\times SDM\times Scen}$, $P_{production,GCM\times SDM\times Scen}$, and $P_{production,CM\times GCM\times SDM\times Scen}$ were the proportions of uncertainty contributed by CM, SDM, GCM, *Scen*, and their interactions, respectively.

3. Results

3.1. Changes of the phenology and grain yield of winter wheat

The parameters estimated and verified with relevant field experiment data (Fig. S2) were used in the six CMs to simulate the phenology dates and per unit yield of winter wheat under various scenarios. Compared with the baseline of 1971–2010 (Table S15), future climate change accelerated the development of winter wheat and reduced the growing days (Fig. 2a, b), which was mainly due to the rise of temperature (Fig. S3a). The mean anthesis dates, which were simulated with the CM ensemble driven by 27 GCMs across the 166 weather stations in the Loess Plateau, were 13 and 20 days earlier in 2041–2060 and

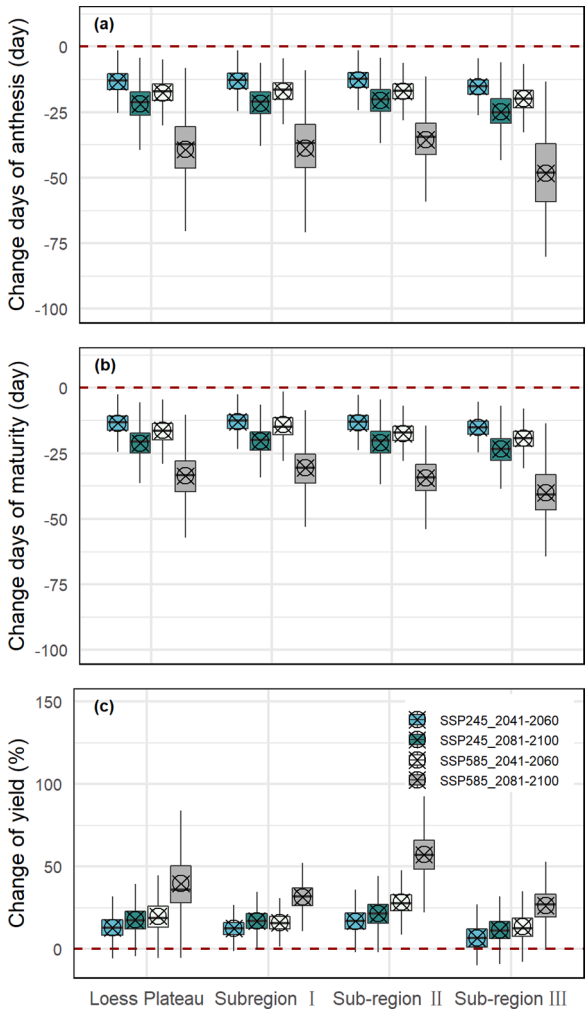

Fig. 2. Projected change days of anthesis (a), days of maturity (b), and per unit yield (c) based on the ensemble crop models (CMs) in 2041–2060 and 2081–2100 under SSP245 and SSP585 scenarios across all of the weather stations in the whole region and the three subregions (Subregion I, II, and III). Data presented are changes of mean values in 2041–2060 and 2081–2100 with the 27 selected global climate models (GCMs) at all of the weather stations compared to the baseline of 1971–2010. In each box, there are 27×166, 27×77, 27×59, 27×30 values corresponding to the 27 selected global climate models (GCMs) and numbers of weather stations in the Loess Plateau, Subregion I, II, and III, respectively. Box boundaries indicate the 25th and 75th percentiles; the black line within the box marks the median; circle with crossed lines marks the mean; whiskers below and above the box indicate the 10th and 90th percentiles, respectively. And the same below.

2081–2100 under SSP245; and 18 and 38 days earlier under SSP585, respectively (Fig. 2a). In addition, the advancing of anthesis dates was greater than the maturity dates in 2081–2100 under SSP585, especially in the phenology simulations with the AquaCrop, DSSAT-CSCRP-Wheat, and DSSAT-NWheat model (Figs. S4a, d, e and S5a, d, e). Although warm regions (Subregions I and II) would become warmer than cold region (Subregions III) (Fig. S3a), changes of life cycle of winter wheat in warm regions were less than those in cold regions under future climate change (Fig. 2b).

Compared with the per unit yield (4343 kg ha^{-1} in Table S15) of the baseline of 1971–2010, most of the 27 GCMs agreed on the rise of per unit yield in future periods across the 166 weather stations in the Loess Plateau. Over the whole region, multi-GCMs mean of CM ensembleprojected yield changes were 12.4% in 2041–2060 and 15.2% in 2081–2100 under SSP245, which were lower than the changes under SSP585, about 17.1% in 2041–2060 and 27.5% in 2081–2100 (Fig. 2c). The wet and warm Subregion II had the largest increase in simulated yields (Fig. 2c). Although yields were projected to increase in the future by most combinations of CMs and GCMs, the magnitudes of yield changes were remarkably different (Fig. S6). Among the six CMs, the DSSAT-NWheat model projected the lowest magnitude of yield changes in the Loess Plateau, since the mean yield change of multi-GCMs projections was 2.7% in 2041–2060 and 5.2% in 2081–2100 under SSP245, and 5.2% in 2041–2060 and 24.6% in 2081–2100 under SSP585 (Fig. S6e). The AquaCrop model projected more than 56.3% yield increase in the future under both SSPs scenarios in the Loess Plateau (Fig. S6b). Additionally, the trends of yield change varied among the six CMs in future period under both SSPs scenarios in the Subregion III. Yield changes were projected to stay at the level of baseline by the DSSAT-CERES-Wheat, DSSAT-NWheat, and STICS models (Fig. S6c, e, f) and to be greater than the baseline by the Apsim, AquaCrop, and DSSAT-CSCRP-Wheat models (Fig. S6a, b, d) in Subregion III.

3.2. *Changes of climate-suitable areas for winter wheat*

Both observed and downscaled weather data from the 27 GCMs were used to drive the multiple SDMs to simulate climate-suitable areas for winter wheat in the Loess Plateau. In the baseline of 1971–2010, climate-suitable areas of winter wheat projected by the SDMs shared the same spatial pattern with the planting areas obtained through remote survey (Jin et al., 2018) (Fig. S7a–j). Temperature-related and rainfall-related variables had relatively lager influences on the SDM-predictions than the rest 17 variables. For example, the variables of PWM (Rainfall of wettest month), MTCM (Minimum temperature of the coldest month), and TR (Temperature range) were the top-3 influential factors and their relative influences were 15.8%, 15.7%, and 12.7% (Fig. S7k), respectively.

Predicted climate-suitable areas by the ensemble-weighted SDMs driven by the 27 GCMs were compared with the predictions in the baseline of 1971–2010. Compared with the spatial distribution of planting areas of winter wheat in the baseline, the spatial distribution was projected to extend northward in Subregion I and westward in Subregion III in 2041–2060 under SSP245, but retract westward in Subregion III in 2041–2060 under SSP585 (Fig. 3a, c). The mean climate-suitable areas based on multi-GCMs projections were predicted to be 3.45 and 3.40 million hectares in 2041–2060 under SSP245 and SSP585, respectively (Table 1). The projected changes of the mean climate-suitable areas were unremarkable under SSP245 (−0.5%) and SSP585 (−2.0%) scenarios in 2041–2060 (Fig. 3e). However, the Loess Plateau would lose about 10.9% and 24.7% of climate-suitable areas for winter wheat under SSP245 and SSP585 in 2081–2100 (Fig. 3e), with projected climate-suitable areas of 3.09 and 2.61 million hectares. The losses of climate suitability mainly occurred in Subregion III (Fig. 3b, d), about −15.0% and −51.1% under SSP245 and SSP585 (Fig. 3e), respectively. In Subregion I, climate-suitable areas for winter wheat would extend northward and retract eastward under SSP245 and SSP585 (Fig. 3b, c), with climate-suitable areas of 1.65 and 1.63 million hectares in 2041–2060 under SSP245 and SSP585, and 1.42 and 1.35 million hectares in 2081–2100 (Table 1). In Subregion II, the changes of climate-suitable areas for winter wheat were remarkable in 2081–2100, about −7.6% and −17.1% under SSP245 and SSP585 (Fig. 3e).

In addition, the changes of climate-suitable areas predicted by the nine SDMs varied under the four climate change scenarios in the Loess Plateau. The GAM model projected unremarkable change in climate-suitable areas under SSP245 and SSP585 in 2041–2060, but the mean climate-suitable areas of multi-GCMs declined about 74.6% and 91.4% under SSP245 and SSP585 in 2081–2100 (Fig. S8a). Compared with the baseline of 1971–2010, the Glmnet, Maxlike, MLP, and RBF models projected reductions in climate-suitable areas in 2041–2060 and 2081–2100 both under SSP245 and SSP585 (Fig. S8c–f). The mean climate-suitable areas projected by the GBM model and multi-GCMs would increase more than 9.6% in the future in the Loess Plateau

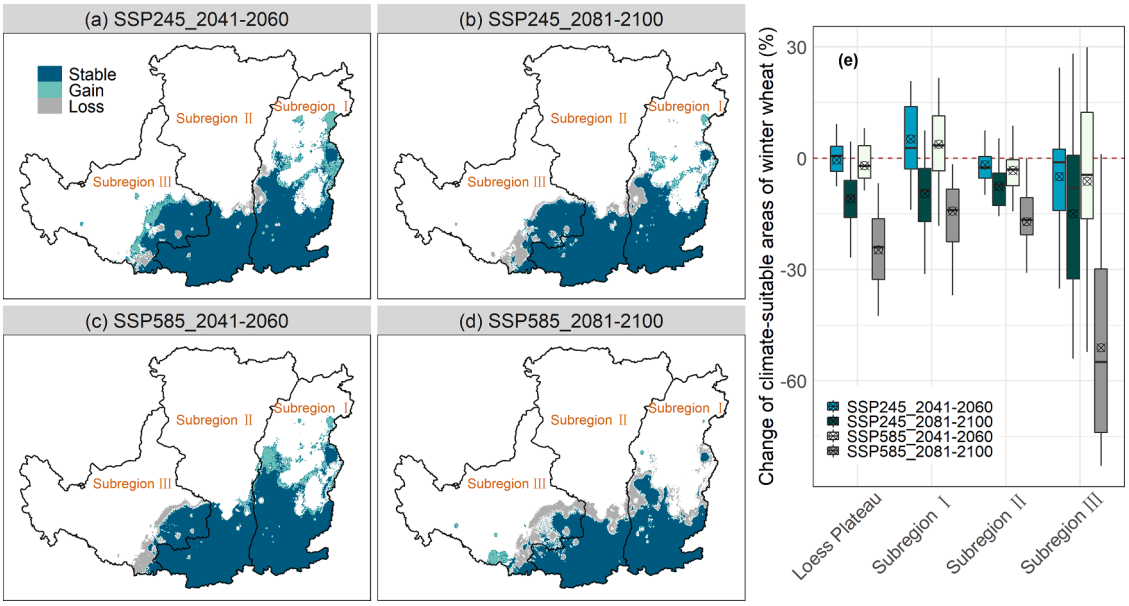

Fig. 3. Spatial distributions of multi-GCM-median climate-suitable areas of winter wheat cultivation projected by the TSS-weighted ensemble of nine species distribution models (SDMs) with 27 GCMs under the SSP245 and SSP585 scenarios in the Loess Plateau of China. Changes of climate-suitable planting areas are presented for the period of 2041–2060 under SSP245 (a), 2081–2100 under SSP245 (b), 2041–2060 under SSP585 (c), and 2081–2100 under SSP585 (d) compared with the baseline of 1971–2010. Cyan pixels represent the areas that would become suitable (or Gain); green pixels the areas that are currently suitable (or Stable); and gray pixels the areas that would become unsuitable (or Loss). Relative changes in climate-suitable areas of winter wheat are projected in the Loess Plateau and three subregions (Subregion I, II, and III) under the SSP245 and SSP585 scenarios (e). The elements of each box are the SDM-predictions with 27 GCMs.

Table 1
Multi-GCM means of projected climate-suitable areas (million hectare) based on the ensemble-weighted SDMs in 2041–2060 and 2081–2100 under SSP245 and SSP585 in the Loess Plateau and three subregions (Subregion I, II, and III), respectively. The SDMs-predicted climate-suitable areas of winter wheat under future climate were adjusted based on the actual areas of winter wheat cultivation in the China Statistical Yearbook (2007–2014) with the correction factor shown in Table s14.

Regions	SSP245 2041–2060	SSP245 2081–2100	SSP585 2041–2060	SSP585 2081–2100
The Loess Plateau	3.45 (2.87–3.93)[a]	3.09 (2.54–3.62)	3.40 (2.67–3.75)	2.61 (1.99–3.24)
Subregion I	1.65 (1.35–1.90)	1.42 (1.08–1.89)	1.63 (1.28–1.91)	1.35 (0.99–1.91)
Subregion II	1.39 (1.28–1.58)	1.31 (1.20–1.50)	1.37 (1.22–1.54)	1.18 (0.74–1.58)
Subregion III	0.47 (0.30–0.61)	0.42 (0.23–0.63)	0.46 (0.23–0.64)	0.24 (0.08–0.64)

[a] The number outside is the mean value and the numbers in the parentheses are the minimum and maximum values.

(Fig. S8b). Compared with the baseline, the predicted climate-suitable areas by the RF, RPART, and SVM models would increase in 2041–2060 both under SSP245 and SSP585, but decline in 2081–2100 under SSP585 (Fig. S8g–i).

3.3. Changes of regional winter wheat production

The per unit yield projected by six CMs and CM ensemble and climate-suitable areas projected by nine SDMs, and TSS weighted-ensemble SDMs driven by 27 GCMs were integrated to project the changes of regional winter wheat production in the Loess Plateau under future climate change. Based on the simulations with CM ensemble, TSS weighted-ensemble SDMs, and 27 GCMs, most GCM projected increases in regional winter wheat production. The mean winter wheat production of multi-GCMs would increase by 14.6% and 19.7% in 2041–2060 and by 4.9% and 3.5% in 2081–2100 under SSP245 and SSP585 (Fig. 4a), which was mainly due to the increases in per unit yield of winter wheat. The mean winter wheat production of multi-GCMs were projected to be 17.66 million tons and 18.20 million tons in 2041–2060 and to be 16.41 million tons and 16.10 million tons in 2081–2100 under SSP245 and SSP585, respectively (Table 2). In addition, the magnitude of changes in winter wheat production varied spatially under the four climate change scenarios (Fig. 4a). Under SSP245, mean winter wheat production of multi-GCMs was projected to increase by 19.0% in 2041–2060 and by 4.5% in 2081–2100 in Subregion I, by 13.7% and 10.3% in Subregion II, and by −0.3% and −12.0% in Subregion III (Fig. 4a). Thus, regional winter wheat production in warm and wet regions (Subregion I and II) could benefit from future climate change. However, future climate change might damage regional winter wheat production in dry and cold Subregion III (Fig. 4a).

Generally, the changes of regional winter wheat production projected by the six CMs with ensemble-SDMs and multi-GCMs were less than 50.0% in 2041–2061 and 2081–2100 both under SSP245 and SSP585 in the Loess Plateau (Fig. S9). Most CMs projected increase in winter wheat production with ensemble-SDMs and multi-GCMs in Subregion II, but the trends of projected winter wheat production varied among of the six CM under the four climate change scenarios in Subregion I and Subregion III (Fig. S9).

However, variations among the nine SDMs could lead to larger differences in temporal and spatial changes of projected winter wheat production (about −52.2%~101.4%, Fig. S10) than the variations among the six CMs. The changes of winter wheat production shared the similar pattern with the change of projected climate-suitable areas (Figs. S7 and S10). In addition, the slopes of linear regressions between changes of regional winter wheat production and changes of per unit yield of winter wheat were less than 0.14, while the slopes between changes of regional winter wheat production and changes of climate-suitable areas for winter wheat were 0.14~0.16 (Fig. 4b, c). These statistics showed that the changes in climate-suitable areas for winter wheat could contribute more to the changes in regional winter wheat production than the changes in per unit yield of winter wheat.

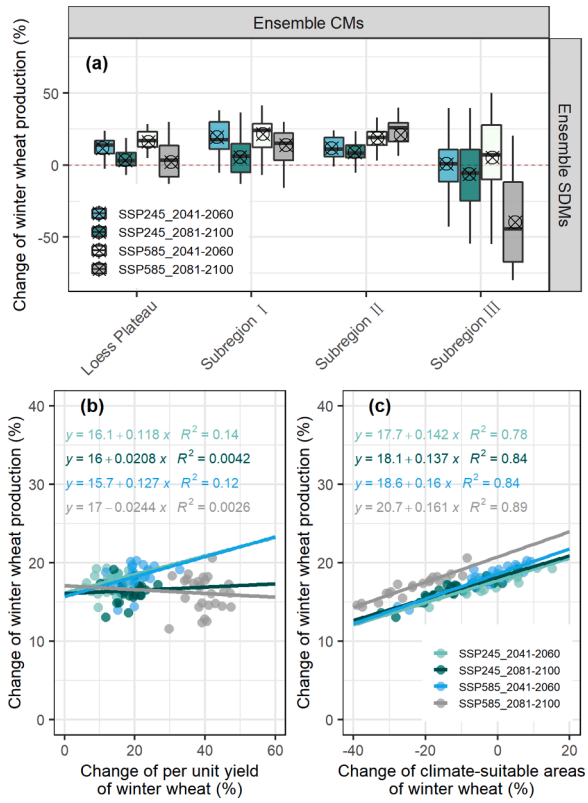

Fig. 4. Changes of regional winter wheat production based on per unit yield projected by ensemble crop models (CMs) and corrected climate-suitable areas projected by weighted-ensemble SDMs driven by 27 GCMs in 2041–2060 and 2081–2100 under the SSP245 and SSP585 scenarios compared to the baseline of 1971–2010 (a); linear regression between the change of winter wheat production and the change of per unit yield of winter wheat (b), and linear regression between the change of winter wheat production and the change of climate-suitable areas of winter wheat (c) in the Loess Plateau. The winter wheat production was the product of the average per unit yield projected by CM ensemble and the climate-suitable areas projected by TSS-weighted ensemble SDMs driven by 27 GCMs under four climate change scenarios in the Loess Plateau and its three subregions. There were 27 projected production values of winter wheat based on the 27 GCMs in each box (a) or under each change scenario (b-c).

3.4. Sources of uncertainties in the projections of yield, climate-suitable areas, and production

The uncertainty sources (i.e. GCMs, CMs, SDMs, *Scen*, and their interactions) in the projections of per unit yield, climate-suitable areas, and production of winter wheat were analyzed through the ANOVA methods (three-way ANOVA for per unit yield and climate-suitable areas; four-way ANOVA for regional production). It was found that CM dominated the projection uncertainties of winter wheat yield in the Loess Plateau and contributed about 38.8% of total uncertainty, which was larger than contributed by the rest six possible sources (Fig. 5a). Emission scenario additionally contributed nearly 36.1% of total uncertainty in the Loess Plateau (Fig. 5a). The uncertainty contributed by emission scenario was 33.9% in Subregion II, which was much higher than those in Subregion I and III. Yield projection uncertainty contributed by CM in Subregion I was more than those in Subregion II and III (Fig. 5a).

The contributions of different sources to the projection uncertainties of climate-suitable area were more uniform than those in per unit yield predictions (Fig. 5b). Among all of the uncertainty sources, the SDM constituted about 25.4% of total uncertainty, followed by the interactions of GCM×SDM, SDM×*Scen*, and SDM×*Scen*×GCM (Fig. 5b). Emission scenario did not contribute much projection uncertainty for climate-suitable areas as for per unit yield. The interactions contributed more projection uncertainty for climate-suitable area (about 15.0% ~25.0%) than for per unit yield (<15.0%) (Fig. 5b). Additionally, the GCM also contributed more projection uncertainty for climate-suitable area (about 10.8%) than for per unit yield (about 2.2%) (Fig. 5b). However, no factor was consistently the dominant source of projection uncertainty of climate-suitable areas in the three subregions. For instance, in Subregion III, the interaction of GCM×SDM contributed the most projection uncertainty for climate-suitable areas among the seven possible sources.

Main factors were no longer the largest uncertainty contributors in the projections of regional winter wheat production in the Loess Plateau, which was different from the projections of per unit yield and climate-suitable areas (Fig. 5c). Interaction of GCM×SDM contributed the largest portion of uncertainty (about 20.9% of total uncertainty) among the 15 possible sources. Generally, the uncertainty contributions in winter wheat production projections by various SDMs varied in different subregions. In particular, the contribution of SDM was surpassed by the interactions of GCM×SDM, SDM×*Scen*×GCM, and SDM×*Scen* in Subregion II. However, SDM was the second largest uncertainty source (about 20.3% of total uncertainty) in the projections of regional winter wheat production under future climate in the Loess Plateau, as well as the largest uncertainty contributor among the four main factors of CM, GCM, *Scen*, and SDM (Fig. 4c). Although uncertainty contributed by SDM increased with numbers of SDM involved in their combinations, SDM was always the largest contributor among four main factors (Fig. S11). Thus, large uncertainty contributed by SDM might not depends on the SDM combinations. Notedly, the portions of uncertainty contributed by SDM and *Scen* in the projections of winter wheat production were similar to those in the projections of climate-suitable areas. Uncertainties contributed by CM were exceeded by *Scen* and GCM, namely CM was the smallest contributor among the four main factors of CM, GCM, *Scen*, and SDM (Fig. 5c). CM contributed about 3.0% of total uncertainty in the projections of regional winter wheat production in the Loess Plateau, which was far smaller than in the projections of per unit yield (Fig. 5a, c). Furthermore, the portion of projection uncertainty contributed by SDM-related factors was about 70.1% and was about 5.3% by CM-related factors. This indicated that the prediction uncertainty of regional winter wheat production was more determined by the projection uncertainty of climate-suitable areas than that by the projection uncertainty of per unit yield of winter wheat (Fig. 5d).

Table 2
Multi-GCM means of projected regional production (million tons) of winter wheat based on the ensemble of crop models and ensemble-weighted SDMs in 2041–2060 and 2081–2100 under SSP245 and SSP585 in the Loess Plateau and the three subregions (Subregion I, II, and III), respectively.

Regions	SSP245		SSP585	
	2041–2060	2081–2100	2041–2060	2081–2100
The Loess Plateau	17.66 (14.28–19.30) [a]	16.40 (13.07–19.13)	18.20 (13.94–20.29)	16.08 (11.58–20.61)
Subregion I	8.56 (6.95–9.79)	7.64 (5.63–9.58)	8.32 (6.43–9.62)	7.81 (10.80–10.36)
Subregion II	7.49 (6.61–9.34)	7.31 (6.34–8.57)	8.16 (7.03–9.14)	8.31 (5.13–10.36)
Subregion III	2.05 (1.22–2.81)	1.91 (1.00–2.80)	2.21 (1.06–3.06)	1.27 (0.41–2.50)

[a] The number outside is the mean value and the numbers in the parentheses are the minimum and maximum values.

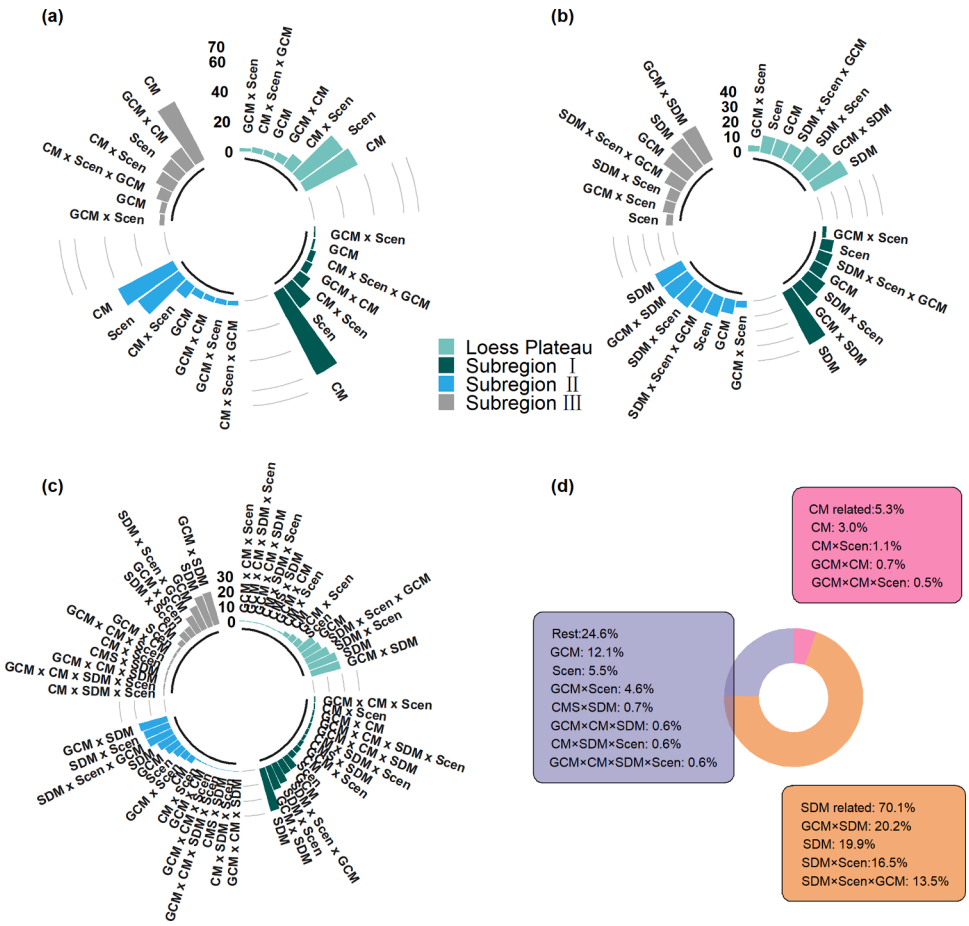

Fig. 5. Contributions of uncertainties (%) in the projections of per unit yield (a), climate-suitable areas (b), and regional production (c) of winter wheat in the Loess Plateau and its three subregions (Subregion I, II, and III). The main contributions to the projection uncertainties of winter wheat production by different contributors were summarized in subplot (d). The uncertainty sources of winter wheat production were dissected into crop simulation model (CM), global climate model (GCM), emission scenario (*Scen*), species distribution model (SDM), and their interactions. Light green, green, light blue, and gray represent the Loess Plateau, Subregion I, and Subregion II, and Subregion III, respectively. In subplot (d), main contributors to the projection uncertainties of winter wheat production in the Loess Plateau were CM-related sources (i.e. CM, GCM×CM, CM×Scen, and GCM×CM×*Scen*; pink box), SDM-related sources (i.e. SDM, SDM×*Scen*, GCM×SDM, and SDM×*Scen*×GCM; orange box), and the rest sources (i.e. *Scen*, GCM, CMS×SDM, GCM×*Scen*, GCM×CM×SDM, CM×SDM×*Scen*, and GCM×CM×SDM×*Scen*; purple box).

4. Discussion

In this study, based on the combinations of CMs, SDMs, and GCMs, we gained a deeper understanding of the spatial and temporal changes of per unit yield, climate-suitable areas, and regional production of winter wheat under future climate change in the Loess Plateau of China. Furthermore, we comprehensively quantified the contributions of different uncertainty resources in the projections of per unit yield, climate-suitable areas, and regional production of winter wheat in this region. For per unit yield projections, there was an increasing trend in spite of a reduction in wheat growth period, which was probably due to the rising in rainfall and CO_2 in wheat growing season (Jägermeyr et al., 2021; Yang et al., 2015). The results of this study (especially in Subregion I and II) were contrary to the decrease trend reported by LV et al. (2013). The discrepancy of crop model, model setting, emission scenarios, and GCMs between the two studies might give rise to the contrary trends for per unit yield. For example, LV et al. (2013) used only one crop model (wheat-grow) driven by three selected GCMs from CMIP3 under A1, A2, and B1 emission scenarios. By contrast, we used six crop models and 27 GCMs. Our projected yield was based on multiple crop model ensemble rather than one individual model. Additionally, there were relative larger bias in phenology simulations reported by LV et al. (2013).

At Changwu of the Loess Plateau, per unit yield of winter wheat was projected to increase by 4.0%–11.2% based on the ensemble-crop-model simulations under the emission scenarios in CMIP5 (Wang et al., 2020). However, their projected increase of per unit yield was lower than that in this study (about 12.4%–27.5%). In the parts of Shaanxi and Gansu province located in the Loess Plateau, Ye et al. (2020) pointed out that potential wheat yield would increase by 5.0%–10.3% based on simulations with ensemble-crop models under +2.0 °C and 487 ppm CO_2 scenario. We found that wheat productivity increased more under CMIP6 than other studies under CMIP5 in the same area as our study (Saddique et al., 2020; Yang et al., 2020; Zheng et al., 2020) This is consistent with the result of Jägermeyr et al. (2021). They reported that global wheat productivity had a higher increase under CMIP6 than that under CMIP5. In addition, the discrepancy of different crop modeling ensembles might be also explained the differences between the projected yields in our research and those in some recent studies.

Despite alteration in the spatial pattern of climate suitability of winter wheat in 2041–2060 under both SSP245 and SSP585 scenarios, climate-suitable areas reduced under the four climate change scenarios in the Loess Plateau. However, Yang et al. (2015) reported that there could be an increase of 80.0% for crop planting areas in 2011–2040 in the Loess Plateau. This contradiction was probably due to the discrepancies of input variables and modeling concepts between Yang et al. (2015) and this study. For instance, cumulative temperature (> 0 °C) was applied by Yang et al. (2015) to estimate crop planting areas in future periods. However, climate suitability of crops depends not only on temperature, but also on precipitation, topography, land use, and etc. (Rana et al., 2020; Wang et al., 2018). He et al. (2019) reported 10.7%, 18.8%, and 14.7% reductions in climate-suitable areas for summer maize cultivation in China at 1.5 °C global warming under RCP2.6, RCP4.5, and RCP8.5, and 17.3% and 14.7% reductions at 2.0 °C global warming under RCP4.5 and RCP8.5. The projected reductions in climate-suitable areas in this study were consistent with the results of He et al. (2019), which was mainly due to the similarity in model variables and concepts. In this study, the main reason for projected reductions in climate-suitable areas was probably the temperature rise,

which was also consistent with the results of He et al. (2019). Similarly, Ramirez-Cabral and Kumar (2016) also suggested that heat was one of the main factors limiting and reducing the distributions of common bean under current and future conditions.

Most of previous related research mainly focused on the projections of per unit grain yield based on simulations with climate-crop models under future climate change. Globally, spatial distributions of crop cultivation areas have changed under recent climate change. Although how climate change affects crop production at different scales (Lobell et al., 2011; Ye et al., 2020) has been discussed, the planting areas of the crops investigated were always assumed to be stable. However, this is not the truth. In this study, we integrated multiple CMs, SDMs, and GCMs to investigate the regional production of winter wheat in the Loess Plateau of China, taking into account the changes of crop climate-suitable areas under future climate change. Most of the simulations based on the combinations of CMs and GCMs agreed on increases in projected per unit yield of winter wheat, but decreases in projected climate-suitable areas for winter wheat under the four climate change scenarios in the Loess Plateau. Generally, current main crop models could correctly simulate the attainable yields of given crops, but they lack delicate descriptions of the responses of crop growth and development to extreme climatic events. This contradiction may contribute to the phenomenon that current crop models might underestimate the influences of extreme weather conditions on crop yield reduction under future climate change (Feng et al., 2019). On the other hand, the SDMs usually worked from the perspective of environment, but lack the feedback mechanism of crops to environment, which may lead to the overestimations of negative impacts of climate change on climatic suitability of crops. Engelhardt and Neuschulz (2020) suggested that potential effects of climate change on future distributions of nutcracker might be overestimated when trophically-interacting plants were ignored in future projections. In addition, the SDMs models are statistical models trained by historical environmental variables, which might limit its ability in future projection when environmental conditions changed. Santini et al. (2021) suggested that the degree of environmental similarity between the present and future environmental conditions was an important predictor for the predictive accuracy of future projections when using SDMs.

Through the analysis of projection uncertainty of regional winter wheat production under future climate change, the contributions by different sources to total uncertainty were quantified in this study. In the Loess Plateau, the interaction of GCM×SDM was identified as the main source of uncertainty in the projections of regional winter wheat production. This was because the projection uncertainty of region winter wheat production was more contributed by the projection uncertainty of climate-suitable areas than by the projection uncertainty of per unit yield of winter wheat. In addition, the uncertainty contributed by GCM in per unit yield predictions could be superposed to the uncertainty contributed by GCM×SDM interaction in climate-suitable areas projections. Consequently, the interaction of GCM×SDM became the dominant uncertainty contributor in the projections of regional winter wheat production. Actually, Thuiller et al. (2019) also found that there was no absolute dominant factor among the SDMs, GCMs and RCPs in uncertainty partitioning of future projections of global biodiversity.

Some previous research based on climate-crop-model method suggested that CM (crop model) dominated the projection uncertainty of grain yield under future climate change in the Loess Plateau. Among the four main factors (i.e. CM, GCM, *Scen*, and SDM), SDM and CM were the largest and smallest uncertainty contributors in the projections of regional winter wheat production with consideration of changes in crop climatic suitability. Generally, CM dominated the projection uncertainty of per unit yield of winter wheat, notwithstanding the changes of per unit yield contributed less to the changes of regional production than the changes of climate-suitable areas of winter wheat (Fig. 3b, c). Furthermore, the projection uncertainties of per unit yield and climate-suitable areas contributed separately by GCM and *Scen* would be superimposed to the projection uncertainty of regional winter wheat production. Finally, SDM was the dominant contributor in projection uncertainty of climate-suitable areas of winter wheat. The ranking of contributors to projection uncertainty of regional winter wheat production was as: SDM > GCM > *Scen* > CM. In other words, CM was relatively certain in the projections of regional winter wheat production taking into account the changes in crop climatic suitability under future climate. In general, the comprehensive uncertainty analysis in this study could help to rationally integrate the modeling method theory of global climate models, crop modeling, and species distribution modeling on the projection of global wheat production under future climate change. However, in future studies, other possible uncertainty resources, including the parameter optimization strategies of CM and SDM models, variable settings of SDM models, determination of '*presences*' and '*absences*', management practice settings in CM models, and etc., should also be considered in the projections of regional winter wheat production with consideration of changes of crop climatic suitability under future climate. Furthermore, different management options in crop models such as changing sowing date, irrigation or fertilize strategy, planting density are likely to affect wheat growth and yield, which may lead to different results in uncertainty analysis and need to be further studied (Xiong et al., 2019).

5. Conclusions

This comprehensive study of winter wheat production projection revealed opposite trends of per unit grain yield and climate-suitable areas of winter wheat under future climate change in the Loess Plateau of China. Although rise in yield per hectares could offset the negative influences of climate change on winter wheat production in the Loess Plateau to some extent, the changes of climate-suitable areas of winter wheat could affect winter wheat production more seriously than the changes of per unit yield. In addition, the uncertainties contributed by the GCMs (Global climate models) in the predictions of per unit yield and climate-suitable areas could be superimposed in the projections of regional winter wheat production under future climate change. Crop models were proved relatively more certain than the GCMs and SDMs (Species distribution models) in the projections of winter wheat production with consideration of the changes of crop climatic suitability in the future.

Declaration of Competing Interest

The authors declare that they have no known competing financial interests or personal relationships that could have appeared to influence the work reported in this paper.

Acknowledgements

This research was supported by the Natural Science Foundation of China (No. 41961124006, 52079115), the Key Research and Development Program of Shaanxi (No. 2019ZDLNY07–03), the "Project Innovation" of the Chinese Academy of Agricultural Sciences (2021–2025, IARRP), the Open Project Fund from the Key Laboratory of Eco-Environment and Meteorology for the Qinling Mountains and Loess Plateau, Shaanxi Provincial Meteorological Bureau (No. 2019Z-5), and the "111 Project" (No. B12007) of China.

We acknowledge the modeling groups, the Program for Climate Model Diagnosis and Intercomparison (PCMDI) and the WCRP's Working Group on Coupled Modelling (WGCM) for their roles in making available the WCRP CMIP6 multi-model dataset. Support of this dataset is provided by the Office of Science, US Department of Energy. Dr. Ian Macadam of the University of New South Wales downloaded the raw GCM monthly data. And Dr. De Li Liu of the NSW Department of Primary Industries used NWAI-WG to downscale downscaled daily data. Also, we thank AGRIVY (www.agrivy.com) for providing us the data for this study.

Supplementary materials

Supplementary material associated with this article can be found, in the online version, at doi:10.1016/j.agrformet.2022.108933.

References

Araújo, M.B., Anderson, R.P., Barbosa, A.M., Beale, C.M., Dormann, C.F., Early, R., Garcia, R.A., Guisan, A., Maiorano, L.N., 2019. Standards for distribution models in biodiversity assessments. Sci. Adv. 5 (1), eaat4858.

Asseng, S., Ewert, F., Martre, P., Rötter, R.P., Lobell, D.B., Cammarano, D., Kimball, B.A., Ottman, M.J., Wall, G.W., White, J.W., Reynolds, M.P., Alderman, P.D., Prasad, P.V. V., Aggarwal, P.K., Anothai, J., Basso, B., Biernath, C., Challinor, A.J., De Sanctis, G., Doltra, J., Fereres, E., Garcia-Vila, M., Gayler, S., Hoogenboom, G., Hunt, L.A., Izaurralde, R.C., Jabloun, M., Jones, C.D., Kersebaum, K.C., Koehler, A.K., Müller, C., Naresh Kumar, S., Nendel, C., O'Leary, G., Olesen, J.E., Palosuo, T., Priesack, E., Eyshi Rezaei, E., Ruane, A.C., Semenov, M.A., Shcherbak, I., Stöckle, C., Stratonovitch, P., Streck, T., Supit, I., Tao, F., Thorburn, P.J., Waha, K., Wang, E., Wallach, D., Wolf, J., Zhao, Z., Zhu, Y., 2015. Rising temperatures reduce global wheat production. Nat. Clim. Change 5 (2), 143–147.

Asseng, S., Ewert, F., Rosenzweig, C., Jones, J.W., Hatfield, J.L., Ruane, A.C., Boote, K.J., Thorburn, P.J., Rötter, R.P., Cammarano, D., Brisson, N., Basso, B., Martre, P., Aggarwal, P.K., Angulo, C., Bertuzzi, P., Biernath, C., Challinor, A.J., Doltra, J., Gayler, S., Goldberg, R., Grant, R., Heng, L., Hooker, J., Hunt, L.A., Ingwersen, J., Izaurralde, R.C., Kersebaum, K.C., Müller, C., Naresh Kumar, S., Nendel, C., O'Leary, G., Olesen, J.E., Osborne, T.M., Palosuo, T., Priesack, E., Ripoche, D., Semenov, M.A., Shcherbak, I., Steduto, P., Stöckle, C., Stratonovitch, P., Streck, T., Supit, I., Tao, F., Travasso, M., Waha, K., Wallach, D., White, J.W., Williams, J.R., Wolf, J., 2013. Uncertainty in simulating wheat yields under climate change. Nat Clim Chang 3 (9), 827–832.

Basso, B., Martinez-Feria, R.A., Rill, L., Ritchie, J.T., 2021. Contrasting long-term temperature trends reveal minor changes in projected potential evapotranspiration in the US Midwest. Nat. Commun. 12 (1), 1476.

Chavez, E., Conway, G., Ghil, M.S., 2015. An end-to-end assessment of extreme weather impacts on food security. Nat. Clim. Change 5 (11), 997–1001.

Corbeels, M., Berre, D., Rusinamhodzi, L.L.R., 2018. Can we use crop modelling for identifying climate change adaptation options? Agric. For. Meteorol. 256-257, 46–52.

Dai, Y., Shangguan, W., Duan, Q., Liu, B., Fu, S.N., 2013. Development of a China dataset of soil hydraulic parameters using pedotransfer functions for land surface modeling. J. Hydrometeorol. 14 (3), 869–887.

Ding, D.Y., Feng, H., Zhao, Y., Liu, W.Z, Chen, H.X., He, J.Q, 2016. Impact assessment of climate change and later-maturing cultivars on winter wheat growth and soil water deficit on the Loess Plateau of China. Climatic Change 138 (1–2), 157–171.

Elith, J.L., John, R., 2009. Species distribution models: ecological explanation and prediction across space and time. Annu. Rev. Ecol. Evol. Syst. 40, 677–697.

Engelhardt, E.K., Neuschulz, E.L.H., 2020. Ignoring biotic interactions overestimates climate change effects: the potential response of the spotted nutcracker to changes in climate and resource plants. J. Biogeogr. 47 (1), 143–154.

Feng, P., Wang, B., Liu, D.L., Waters, C., Xiao, D., Shi, L.Y., 2020. Dynamic wheat yield forecasts are improved by a hybrid approach using a biophysical model and machine learning technique. Agric. For. Meteorol. 285-286, 107922.

Feng, P., Wang, B., Liu, D.L., Waters, C.Y., 2019. Incorporating machine learning with biophysical model can improve the evaluation of climate extremes impacts on wheat yield in south-eastern Australia. Agric. For. Meteorol. 275, 100–113.

Gidden, M.J., Riahi, K., Smith, S.J., Fujimori, S., Luderer, G., Kriegler, E., van Vuuren, D. P., van den Berg, M., Feng, L., Klein, D., Calvin, K., Doelman, J.C., Frank, S., Fricko, O., Harmsen, M., Hasegawa, T., Havlik, P., Hilaire, J., Hoesly, R., Horing, J., Popp, A., Stehfest, E., Takahashi, K., 2019. Global emissions pathways under different socioeconomic scenarios for use in CMIP6: a dataset of harmonized emissions trajectories through the end of the century. Geosci. Model Dev. 12 (4), 1443–1475.

He, L., Asseng, S., Zhao, G., Wu, D., Yang, X., Zhuang, W., Jin, N.Y., 2015. Impacts of recent climate warming, cultivar changes, and crop management on winter wheat phenology across the Loess Plateau of China. Agric. For. Meteorol. 200, 135–143.

He, L., Cleverly, J., Chen, C., Yang, X., Li, J., Liu, W.Y., 2014. Diverse responses of winter wheat yield and water use to climate change and variability on the semiarid Loess Plateau in China. Agron. J. 106 (4), 1169–1178.

He, Q.Z., 2016. Climate-associated distribution of summer maize in China from 1961 to 2010. Agric. Ecosyst. Environ. 232, 326–335.

He, Q., Zhou, G., Lü, X.Z., 2019. Climatic suitability and spatial distribution for summer maize cultivation in China at 1.5 and 2.0 °C global warming. Sci. Bull. 64 (10), 690–697.

IPCC, 2019. 2019: Climate Change and Land: an IPCC special report on climate change, desertification, land degradation, sustainable land management, food security, and greenhouse gas fluxes in terrestrial ecosystems [P.R. Shukla, J. Skea, E. Calvo Buendia, V. Masson-Delmotte, H.-O. Pörtner, D. C. Roberts, P. Zhai, R. Slade, S. Connors, R. van Diemen, M. Ferrat, E. Haughey, S. Luz, S. Neogi, M. Pathak, J. Petzold, J. Portugal Pereira, P. Vyas, E. Huntley, K. Kissick, M. Belkacemi, J. Malley, (eds.)]. In press.

Jägermeyr, J., Müller, C., Ruane, AC., Elliott, J., Balkovic, J., Castillo, O., Faye, B., Foster, I., Folberth, C., Franke, JA., Fuchs, K., Guarin, JR., Heinke, J., Hoogenboom, G., Iizumi, T., Jain, AK., Kelly, D., Khabarov, N., Lange, S., Lin, T.-S., Liu, W., Mialyk, O., Minoli, S., Moyer, EJ., Okada, M., Phillips, M., Porter, C., Rabin, SS., Scheer, C., Schneider, JM., Schyns, JF., Skalsky, R., Smerald, A., Stella, T., Stephens, H., Webber, H., Zabel, F.R., 2021. Climate impacts on global agriculture emerge earlier in new generation of climate and crop models. Nat. Food 2 (11), 873–885.

Jin, N., Ren, W., Tao, B., He, L., Ren, Q., Li, S., Yu, Q., 2018. Effects of water stress on water use efficiency of irrigated and rainfed wheat in the Loess Plateau, China. Sci. Total Environ. 642, 1–11.

King, M., Altdorff, D., Li, P., Galagedara, L., Holden, J., Unc, A., 2018. Northward shift of the agricultural climate zone under 21(st)-century global climate change. Sci. Rep. 8 (1), 7904.

Lesk, C., Rowhani, P., Ramankutty, N., 2016. Influence of extreme weather disasters on global crop production. Nature 529 (7584), 84–87.

Lesk, C., Coffel, E.H., 2020. Net benefits to US soy and maize yields from intensifying hourly rainfall. Nat. Clim. Change 10 (9), 819–822.

Li, Y., Guan, K., Schnitkey, G.D., DeLucia, E., Peng, B., 2019. Excessive rainfall leads to maize yield loss of a comparable magnitude to extreme drought in the United States. Glob. Change Biol. 25 (7), 2325–2337.

Liu, Z., Ying, H., Chen, M., Bai, J., Xue, Y., Yin, Y., Batchelor, WD., Yang, Yi, Bai, Z., Du, M., Guo, Y., Zhang, Q., Cui, Z., Zhang, F.D., 2021. Optimization of China's maize and soy production can ensure feed sufficiency at lower nitrogen and carbon footprints. Nat. Food 2 (6), 426–433.

Liu, D.L., Zuo, H.P., 2012. Statistical downscaling of daily climate variables for climate change impact assessment over New South Wales, Australia. Climatic Change 10 (9), 819–822.

Lobell, D.B., Schlenker, W., Costa-Roberts, J., 2011. Climate trends and global crop production since 1980. Science 333 (6042), 616–620.

LV, Z.F., Liu, X.J., Cao, W.X., Zhu, Y., 2013. Climate change impacts on regional winter wheat production in main wheat production regions of China. Agric. For. Meteorol. 171-172, 234–248.

Manners, R., Varela-Ortega, C.E., 2020. Protein-rich legume and pseudo-cereal crop suitability under present and future European climates. Eur. J. Agron. 113, 125974.

Naimi, B.A., Miguel, B., 2016. sdm: a reproducible and extensible R platform for species distribution modelling. Ecography 39 (4), 368–375.

Ortiz-Bobea, A., Ault, TR., Carrillo, C.M., Chambers, R.G., Lobell, D.B., 2021. Anthropogenic climate change has slowed global agricultural productivity growth. Nat. Clim. Change 11 (4), 306–312.

Pei, X.X., Dang, J.Y, Zhang, D.Y., Wang, A.J., Zhang, J., Dong, F., 2017. Impact of sowing date on yield and water use efficiency of wheat in different precipitation years in dryland of South Shanxi. Chinese Journal of Eco-Agriculture 25 (4), 553–562.

Ramirez-Cabral, N.Y.Z., Kumar, L.T., 2016. Crop niche modeling projects major shifts in common bean growing areas. Agric. For. Meteorol. 218-219, 102–113.

Rana, S.K., Rana, H.K., Luo, D.S., 2020. Estimating climate-induced 'Nowhere to go' range shifts of the Himalayan Incarvillea Juss. using multi-model median ensemble species distribution models. Ecol. Indic., 107127

Ruan, H., Feng, P., Wang, B., Xing, H., O'Leary, G.J., Huang, Z., Guo, H.L., 2018. Future climate change projects positive impacts on sugarcane productivity in southern China. Eur. J. Agron. 96, 108–119.

Saddique, Q., Liu, D.L., Wang, B., Feng, P., He, J., Ajaz, A., Ji, J., Xu, J., Zhang, C.C., 2020. Modelling future climate change impacts on winter wheat yield and water use: a case study in Guanzhong Plain, northwestern China. Eur. J. Agron. 119, 126113.

Santini, L., Benítez-López, A., Maiorano, L., Čengić, M.H., Mark, A.J., 2021. Assessing the reliability of species distribution projections in climate change research. Divers. Distrib. 27 (6), 1035–1050.

Senapati, N., Brown, H.E.S., Mikhail, A., 2019. Raising genetic yield potential in high productive countries: designing wheat ideotypes under climate change. Agric. For. Meteorol. 271, 33–45.

Stoklosa, J., Daly, C., Foster, S.D., Ashcroft, M.B.W., David, I., 2015. A climate of uncertainty: accounting for error in climate variables for species distribution models. Methods Ecol. Evol. 6 (4), 412–423.

Sun, J., Zhou, G.S., 2012. Climatic suitability of the distribution of the winter wheat cultivation zone in China. Eur. J. Agron. 43, 77–86.

Tanaka, A., Takahashi, K., Masutomi, Y., Hanasaki, N., Hijioka, Y., Shiogama, H.Y., 2015. Adaptation pathways of global wheat production: importance of strategic adaptation to climate change. Sci. Rep. 5 (1), 1–10.

Tao, F., Rotter, R.P., Palosuo, T., Gregorio Hernandez Diaz-Ambrona, C., Minguez, M.I., Semenov, M.A., Kersebaum, K.C., Nendel, C., Specka, X., Hoffmann, H., Ewert, F., Dambreville, A., Martre, P., Rodriguez, L., Ruiz-Ramos, M., Gaiser, T., Hohn, J.G., Salo, T., Ferrise, R., Bindi, M., Cammarano, D., Schulman, A.H., 2018. Contribution of crop model structure, parameters and climate projections to uncertainty in climate change impact assessments. Glob. Change Biol. 24 (3), 1291–1307.

Thuiller, W., Gueguen, M., Renaud, J., Karger, D.N., Zimmermann, N.E., 2019. Uncertainty in ensembles of global biodiversity scenarios. Nat. Commun. 10 (1), 1446.

van Dijk, M., Morley, T., Rau, M.L.S., 2021. A meta-analysis of projected global food demand and population at risk of hunger for the period 2010–2050. Nat. Food 2 (7), 494–501.

Wang, B., Liu, L., O'Leary, G.J., Asseng, S., Macadam, I., Lines-Kelly, R., Yang, X., Clark, A., Crean, J., Sides, T., Xing, H., Mi, C., Yu, Q., 2018. Australian wheat production expected to decrease by the late 21st century. Glob. Change Biol. 24 (6), 2403–2415.

Wang, B., Feng, P., Liu, D.L., O'Leary, G.J., Macadam, I., Waters, C., Asseng, S., Cowie, A., Jiang, T., Xiao, D., Ruan, H., He, J.Y., 2020. Sources of uncertainty for wheat yield projections under future climate are site-specific. Nat. Food 1 (11), 720–728.

Wang, B., Liu, DeLi, Asseng, S., Macadam, IYu, 2017. Modelling wheat yield change under CO_2 increase, heat and water stress in relation to plant available water capacity in eastern Australia. Eur. J. Agron. 90, 152–161.
Wheeler, T.B., 2013. Climate change impacts on global food security. Science 341 (6145), 508–513.
White, JC., Gardea-Torresdey, J., 2018. Achieving food security through the very small. Nat. Nanotechnol. 13 (8), 627–629.
Wieder, W.R., Boehnert J., BonanLangseth G.B., M., 2014. Regridded Harmonized World Soil Database v1.2. Data set. Available on-line [http://daac.ornl.gov] from Oak Ridge National Laboratory Distributed Active Archive Center. Oak Ridge, Tennessee, USA. 10.3334/ORNLDAAC/1247.
Xiao, D., Liu, D.L., Wang, B., Feng, P.W., 2020. Designing high-yielding maize ideotypes to adapt changing climate in the North China Plain. Agric. Syst. 181, 102805.
Xiong, W., Asseng, S., Hoogenboom, G., Hernandez-Ochoa, I., Robertson, R., Sonder, K., Pequeno, D., Reynolds, M.G., 2019. Different uncertainty distribution between high and low latitudes in modelling warming impacts on wheat. Nat. Food 1 (1), 63–69.
Yang, X., Chen, Fu, Lin, X., Liu, Z., Zhang, H., Zhao, J., Li, K., Ye, Q., Li, Y., Lv, S., Yang, P., Wu, W., Li, Z., Lal, R.T., 2015. Potential benefits of climate change for crop productivity in China. Agric. For. Meteorol. 208, 76–84.
Yang, X., Li, Z., Cui, S., Cao, Q., Deng, J., Lai, X.S., 2020. Cropping system productivity and evapotranspiration in the semiarid Loess Plateau of China under future temperature and precipitation changes: an APSIM-based analysis of rotational vs. continuous systems. Agric. Water Manag. 229, 105959.
Yao, N., Zhou, Y.G., Song, L.B., Liu, J., Li, Y., Wu, S.F., Feng, H., He, J.Q., 2015. Parameter estimation and verification of DSSAT-CERES-Wheat model for simulation of growth and development of winter wheat under water stresses at different growth stages. Transactions of the Chinese Society of Agricultural Engineering 31 (12), 138–149.
Ye, Zi, Qiu, X., Chen, J., Cammarano, D., Ge, Z., Ruane, AC., Liu, L., Tang, L., Cao, W., Liu, B.Z., 2020. Impacts of 1.5 °C and 2.0 °C global warming above pre-industrial on potential winter wheat production of China. Eur. J. Agron. 120, 126149.
Zhao, C.Z., Chuang, L., B Liu, B., Piao, SlP, Shilong, W., Xh Wang, X., Lobell, D.L., Huang, D.B., Huang, Y., Yao, H., Huang, M., Mengtian, Y., Yt Yao, Y., Bassu, S.B., SimonaCiais, P.C., 2017. Temperature increase reduces global yields of major crops in four independent estimates. Proc. Natl. Acad. Sci. U. S. A. 114 (35), 9326.
Zhao, C., Piao, S., Huang, Y., Wang, X., Ciais, P., Huang, M., Zeng, Z., Peng, S., 2016. Field warming experiments shed light on the wheat yield response to temperature in China. Nat. Commun. 7, 13530.
Zheng, Z., Cai, H., Wang, Z.W., 2020. Simulation of climate change impacts on phenology and production of winter wheat in Northwestern China using CERES-wheat model. Atmosphere (Basel) 11 (7), 681.